Photonic Network Communications
https://doi.org/10.1007/s11107-018-0776-6

ORIGINAL PAPER

160 Gb/s photonic crystal semiconductor optical amplifier-based all-optical logic NAND gate

Amer Kotb[1,2] · Kyriakos E. Zoiros[3] · Chunlei Guo[1,4]

Received: 12 February 2018 / Accepted: 25 May 2018
© Springer Science+Business Media, LLC, part of Springer Nature 2018

Abstract
The performance of an ultra-fast all-optical logic NOT-AND gate using photonic crystal semiconductor optical amplifiers (PCSOA)-based Mach–Zehnder interferometers is numerically analysed and investigated. The dependence of the quality factor (Q-factor) on the input signals' and PCSOA operating parameters is examined, with the impact of amplified spontaneous emission included so as to obtain realistic results. The achieved Q-factor is 18 at 160 Gb/s, which is higher than when using conventional SOAs.

Keywords 160 Gb/s · All-optical NOT-AND (NAND) gate · Photonic crystal semiconductor optical amplifier · Mach–Zehnder interferometer

1 Introduction

In recent years, intense efforts have improved the performance and scaled the bandwidth of high capacity fibre communication networks by relying on functionalities executed entirely in the optical domain, thus obviating the complications of optoelectronic conversions [1]. All-optical logic gates (AOLGs) are key enabling modules in this context and can be implemented by exploiting the nonlinearities that manifest inside semiconductor optical amplifiers (SOAs). Compared to other technological options, SOAs feature stronger nonlinearity, smaller footprint, better power efficiency, and easier assembly into integration platforms. However, due to SOAs long response time [2–8], it is quite challenging to extend the operation speed of SOA-based logic schemes so as to conveniently keep up with modern single channel data rates [9–11]. On the other hand, the photonic crystal (PC) is a dielectric material, which when incorporated in photonic devices allows the latter to exhibit faster dynamic response and thus being amenable for supporting ultra-high-speed all-optical operation. Additionally, PCs present a reduction in absorption loss, suppression of undesirable nonlinear effects, low power consumption, and high power transmission over other nonlinear structures. This means that if these advantages were combined with those of SOAs, then it would be possible to improve the performance of AOLGs at data rates beyond the limited capability of SOAs. In fact, a PC waveguide in SOA is presented in [12–15], while the design of AOLGs using PCSOAs is the subject of [16,17]. However, these PCSOA-based AOLG demonstrations do not include the NOT-AND (NAND) gate, which nevertheless constitutes a universal gate and hence plays a catalytic role in accomplishing all-optical digital signal processing at both fundamental and system oriented level. In fact, by allowing to synthesize any Boolean function with reduced hardware complexity [18], it forms the core building block in applications such as combinational [19] and sequential photonic logic circuits [20], optical time division multiplexing (OTDM) packet-level synchronization [21], and programmable logic units [22]. Motivated by NAND's outmost significance, in this paper we focus on the theoretical study of the performance of a PCSOA-based all-optical NAND gate. To the best of our knowledge, the implementation of the specific gate has so far not been

✉ Amer Kotb
amer@ciomp.ac.cn

1 The Guo China-US Photonics Laboratory, Changchun Institute of Optics, Fine Mechanics, and Physics, Chinese Academy of Sciences, Changchun 130033, China

2 Department of Physics, Faculty of Science, University of Fayoum, Fayoum 63514, Egypt

3 Lightwave Communications Research Group, Department of Electrical and Computer Engineering, School of Engineering, Democritus University of Thrace, 67100 Xanthi, Greece

4 The Institute of Optics, University of Rochester, Rochester, NY 14627, USA

Published online: 13 June 2018

addressed using PCSOAs, but only conventional SOAs [23–31]. In this manner, we uniquely contribute to this research subject by filling the gap in the existing literature and extending the suite of distinct logic operations that can be executed on two binary input variables [32], using PCSOAs technology. The PCSOAs are embedded in the Mach–Zehnder interferometer (MZI) by being symmetrically placed in its arms. The MZI is an attractive and effective configuration for achieving a variety of optical functions in a photonic optical waveguide circuit owing to its compact architecture, reasonable switching energy requirement, and potential for ultra-high-speed operation [9]. The dependence of the quality factor (Q-factor) on the input signals' and PCSOAs characteristics is numerically analysed and investigated with the impact of amplified spontaneous emission (ASE) included so as to obtain realistic results. The outcome of this novel study confirms that the realization of the NAND gate is feasible with the proposed PCSOA-assisted MZI scheme at 160 Gb/s, with both logical correctness and higher Q-factor than if using conventional SOAs.

This paper is organized as follows: The PCSOA modelling is formulated in Sect. 2. The operation principle and the simulation procedure and results of the NAND gate are described in Sect. 3. Finally, Sect. 4 contains the concluding remarks.

2 PCSOA modelling

By taking into account the interband and the intraband nonlinear effects, which include carrier depletion recombination (CD), carrier heating (CH), and spectral hole burning (SHB), the time-dependent gain for each PCSOA is described by the following coupled equations [17]:

$$\frac{\mathrm{d}h_{\mathrm{CD}}(t)}{\mathrm{d}t} = \frac{h_0 - h_{\mathrm{CD}}(t)}{\tau_{\mathrm{C}}} - (Rv_{\mathrm{g}})h_{\mathrm{PC}}[t] - (\exp[h_{\mathrm{CD}}(t) + h_{\mathrm{CH}}(t) + h_{\mathrm{SHB}}(t)] - 1)\frac{P(t)}{E_{\mathrm{sat}}} \quad (1)$$

$$\frac{\mathrm{d}h_{\mathrm{PC}}(t)}{\mathrm{d}t} = \left(\frac{LR}{\tau_{\mathrm{c}}}\right)(h_0 - h_{\mathrm{PC}}(t)) - \left(Rv_{\mathrm{g}}\right)h_{\mathrm{CD}}(t) \quad (2)$$

$$\frac{\mathrm{d}h_{\mathrm{CH}}(t)}{\mathrm{d}t} = -\frac{h_{\mathrm{CH}}(t)}{\tau_{\mathrm{CH}}} - \frac{\varepsilon_{\mathrm{CH}}}{\tau_{\mathrm{CH}}}(\exp[h_{\mathrm{CD}}(t) + h_{\mathrm{CH}}(t) + h_{\mathrm{SHB}}(t)] - 1)P(t) \quad (3)$$

$$\frac{\mathrm{d}h_{\mathrm{SHB}}(t)}{\mathrm{d}t} = -\frac{h_{\mathrm{SHB}}(t)}{\tau_{\mathrm{SHB}}} - \frac{\varepsilon_{\mathrm{SHB}}}{\tau_{\mathrm{SHB}}}(\exp[h_{\mathrm{CD}}(t) + h_{\mathrm{CH}}(t) + h_{\mathrm{SHB}}(t)] - 1)P(t) - \frac{\mathrm{d}h_{\mathrm{CD}}(t)}{\mathrm{d}t} - \frac{dh_{\mathrm{CH}}(t)}{dt} \quad (4)$$

where functions 'h' represent the PCSOA's gain integrated over its length for CD, PC, CH, and SHB, respectively. In particular, one-dimensional Eq. (2) describes the SOA gain response to the pulse propagation inside the embedded PC waveguide (see Fig. 1) with the heuristic inclusion of the group velocity [12]. $h_0 = \ln[G_0]$, where G_0 is the unsaturated power gain being directly proportional to the injection current I [12]. E_{sat} is the saturation energy, which is related to the saturation power (P_{sat}) through $E_{\mathrm{sat}} = P_{\mathrm{sat}}\,\tau_{\mathrm{c}}$, where τ_{c} is the carrier lifetime. $P(t)$ denotes the power inserted into the PCSOAs. τ_{CH} and τ_{SHB} are the temperature relaxation rates, and $\varepsilon_{\mathrm{CH}}$ and $\varepsilon_{\mathrm{SHB}}$ are the nonlinear gain suppression factors due to CH and SHB, respectively. R is the radiation loss. v_{g} is the light group velocity, i.e. $v_{\mathrm{g}} = c/n_{\mathrm{g}}$, where c is the speed of light in a vacuum and n_{g} is the group index of the semiconductor material. Typically, $L = 300\ \mu\mathrm{m}$, $R = 30\ \mathrm{cm}^{-1}$, and $n_{\mathrm{g}} = 3$ for a standard SOA, while $L = 10\ \mu\mathrm{m}$, $R = 1500\ \mathrm{cm}^{-1}$, and $n_{\mathrm{g}} = 100$ for a PCSOA [12,17]. The total output gain of each PCSOA is given by:

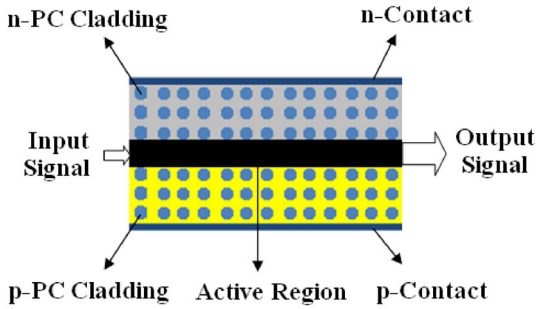

Fig. 1 Schematic diagram of PCSOA's slab waveguide

$$G(t) = \exp[h_{\mathrm{CD}}(t) + h_{\mathrm{CH}}(t) + h_{\mathrm{SHB}}(t)] \quad (5)$$

The schematic diagram of the PCSOA's slab waveguide is illustrated in Fig. 1. The semiconductor materials used in this study are GaInAsP/InP, which should be direct band and lattice matched. The holes are shown passing vertically through the waveguide structure. The PC has a lattice constant of 480 nm, a radius of 158 nm, and a depth of 2.3 μm. The vertical spacing between rows is adjusted to 420 nm [33]. The PCSOA is suitable for optical signal preamplification, switching, and local loss compensation, with output powers, typically ranging from − 10 to 0 dBm [12].

The induced phase change inside the PCSOAs is given by [23]:

$$\Phi(t) = -0.5[\alpha h_{\mathrm{CD}}(t) + \alpha_{\mathrm{CH}}h_{\mathrm{CH}}(t) + \alpha_{\mathrm{SHB}}h_{\mathrm{SHB}}(t)] \quad (6)$$

where α is the traditional linewidth enhancement factor associated with interband carrier dynamics and α_{CH} is the linewidth enhancement factor due to CH, while $\alpha_{\mathrm{SHB}} = 0$ is null because the SHB produces a nearly asymmetrical spectral hole centred at the wavelength of the input signal [34–36].

In this simulation, the pulses contained in data signals A and B are assumed to be Gaussian-shaped whose power

profiles are described by the formula [23]:

$$P_{\mathrm{A,\,B}}(t) = \sum_{n=-\infty}^{n=+\infty} a_{\mathrm{nA,B}} \frac{2\sqrt{\ln(2)}E_0}{\sqrt{\pi}\,\tau_{\mathrm{FWHM}}} \times \exp\left(-\frac{4\ln(2)(t-nT)^2}{\tau_{\mathrm{FWHM}}^2}\right) \quad (7)$$

where $\alpha_{\mathrm{nA,B}}$ is the nth pulse, which takes the logical values of '1' or '0' with equal probability, inside an optical pseudo-random binary sequence (PRBS) [37] of word-length $2^7 - 1$, pulse period (T), full width at half maximum (FWHM) pulse width (τ_{FWHM}), and pulse energy (E_0). Throughout the simulation, the average launched powers of signals A, B, and CW are 0.2, 0.3, and 0.05 mW, respectively [18].

3 NAND

3.1 Operation principle

In this work, the NAND operation is obtained using a serial combination of AND and INVERT gates, similar to Refs. [27–29]. Figure 2 shows the schematic diagram and truth table of the NAND gate with PCSOA-assisted MZIs. The first MZI serves as an AND gate, and the second MZI serves as a NOT (INVERT) gate. For AND operation, data signal A (centred at wavelength λ_1) is inserted through input port 1 into MZI1. Concurrently, data signal B (centred at a different wavelength λ_2) is split by a 3 dB optical coupler (OC) placed at input port 3 into two identical copies, which are inserted into MZI1 both arms. When B = '0', there is no light on which to imprint any perturbation of the initially balanced MZI1 and transfer it at output port 4. Thus, MZI1 is disabled regardless of the binary content of A. This situation changes when B = '1', namely when data sequence B contains a pulse. In this case, the logic result at port 4 depends on the existence or not of a pulse in the same bit slot of data A. More specifically, if A = '0', there is no phase difference created between the two arms of MZI1, which remains balanced by carefully adjusting the injection currents and phase shifters located at each MZI1 branch. Thus, signal B is minimized at port 4, resulting in logical '0' at MZI1 exit. But if A = '1', the phase balance of signal B is broken due to the cross-phase modulation nonlinear effect that manifests in PCSOA1 and which induces a phase shift on signal B travelling in MZI1 upper arm compared to its counterpart in the lower arm. As a consequence, a relative phase difference is created between these components, which if it is made equal to π, then they interfere constructively at port 4 giving a logical '1'. Because the gain that is perturbed by signal A and suffered by signal B recovers only partially before the arrival of the next pulse of signal B, this means that when signal A is 'off', the replicas of signal B may still undergo a differential phase change, which, however, is undesirable as it would produce an erroneous binary result. For this reason, a continuous wave (CW) signal is coupled into MZI1 from input port 2. The role of this auxiliary signal is to sufficiently drop the PCSOA2 gain from the unsaturated state and bring it to the same level as that of PCSOA1 when the latter is not excited by signal A. In this manner, the gain mismatch between the MZI1 arms is compensated and the corresponding induced phase shifts are mutually cancelled, thereby extinguishing the MZI1 output, as pursued. According to this mode of operation, MZI1 yields a pulse, i.e. '1', at output port 4 if and only if a pulse is present in both signals A and B, i.e. A, B = '1, 1', while no pulse appears therein, i.e. '0', if a pulse is absent from either A or B or from both of them, i.e. A, B = '0, 0', '0, 1' or '1, 0', respectively. These combinations of logical pairs and their outcome form the truth table of the Boolean AND logic executed between A and B, i.e. 'A AND B'.

An optical band-pass filter (OBPF) placed at the exit of the AND gate rejects the spectral components other than the switched signal. The AND output sequence, which is centred at λ_2, is amplified by an erbium-doped fibre amplifier (EDFA) and forwarded as 'data' to the MZI2 upper arm through port 5.

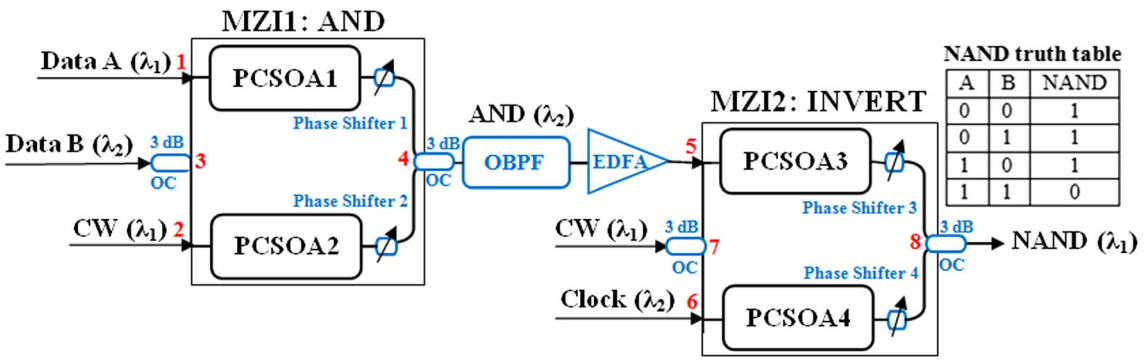

Fig. 2 Schematic diagram and truth table of NAND operation with PCSOAs–MZIs. OBPF: optical band-pass filter. EDFA: erbium-doped fibre amplifier. OC: 3 dB optical coupler

Table 1 Calculation parameters

Symbol	Definition	Value	Unit
E_0	Pulse energy	0.03	pJ
G_0	Unsaturated gain	30	dB
I	Injection current	10	mA
τ_c	Carrier lifetime	20	ps
τ_{FWHM}	Pulse width	1	ps
P_{sat}	Saturation power	25	mW
α	Traditional linewidth enhancement factor	6	
α_{CH}	Linewidth enhancement factor due to CH	1	
α_{SHB}	Linewidth enhancement factor due to SHB	0	
τ_{CH}	Temperature relaxation rate	0.3	ps
τ_{SHB}	Carrier–carrier scattering rate	0.1	ps
ε_{CH}	Nonlinear gain suppression factor due to CH	0.02	W^{-1}
ε_{SHB}	Nonlinear gain suppression factor due to SHB	0.02	W^{-1}
n_g	Group index	100	
L	Length of active region	10	μm
w	Width of active region	2	μm
d	Thickness of active region	0.4	μm
R	Radiation loss	1500	cm^{-1}
Γ	Confinement factor	0.3	
κ	Conversion factor	1×10^{-24}	$W \cdot m^3$

A train of continuous pulses, i.e. clock, with the same pulse shape and intensity is injected from port 6 into the MZI2 lower arm, while a CW light is injected into the MZI2 middle arm. In this way, the exclusive disjunction operation is executed between the data streams injected from MZI2 ports 5 and 6, which according to Boolean algebra laws is equivalent to 'INVERT (A AND B)' or 'A NAND B', whose logic outcome is obtained at output port 8.

3.2 Simulation

The output of the AND gate is described by the following equation:

$$P_{AND}(t) = 0.25P_B(t)\{G_1(t) + G_2(t) - 2\sqrt{G_1(t)G_2(t)}\cos[\Phi_1(t) - \Phi_2(t)]\} \quad (8)$$

while that of the NAND gate by:

$$P_{NAND}(t) = 0.25P_{CW}\{G_3(t) + G_4(t) - 2\sqrt{G_3(t)G_4(t)}\cos[\Phi_3(t) - \Phi_4(t)]\} \quad (9)$$

where $P_B(t)$ and P_{CW} stand for the powers of input signals B and CW, respectively. $G(t)$ and $\Phi(t)$ are the time-dependent gains and induced phase shifts at the corresponding MZIs arms. The simulation has been conducted with the help of Mathematica®. The default values of the critical parameters used in the calculations are cited in Table 1 [31,38,39].

The performance of the NAND gate has been evaluated by means of the Q-factor. This metric is defined as $Q = (S_1 - S_0)/(\sigma_1 + \sigma_0)$, where $S_{1,0}$ is the average and $\sigma_{1,0}$ the standard deviation, respectively, of the expected '1's and '0's photon density, which is linked to the corresponding power through the conversion factor $\kappa = \hbar \upsilon v_g \sigma / \Gamma$, where $\hbar$ is the normalized Planck's constant, υ is the optical frequency, and $\sigma = wd$ is the cross section of the PCSOA active region of width w, thickness d, and confinement factor Γ, i.e. $P(t) = \kappa S(t)$. Figure 3c, d shows the logical outcome and associated eye diagram, respectively, of the NAND operation, which is executed at 160 Gb/s between data signals A (Fig. 3a) and B (Fig. 3b). The all-optical NAND gate is realized with both logical correctness and high quality, i.e. with no pattern effects observed. The calculated Q-factor using the PCSOA-based MZIs is 18, which is rather high compared to what it has previously been reported with standard SOA-based MZIs [7,26,28,29], and well above the lower limit of 6 required to keep the bit error rate less than 10^{-9} [23]. Furthermore, Fig. 4 shows that the specific Q-factor value can be obtained for input signals' finite extinction ratio of 20 dB. This ER magnitude is technologically achievable for pulses having the form, and being as fast and short, as in this paper, at the price of using more complex OTDM pulse generation systems and tighter operating conditions [40,41] than for a much lower ER. The latter would result too in an acceptable Q-factor, as observed from Fig. 4; however, it would also

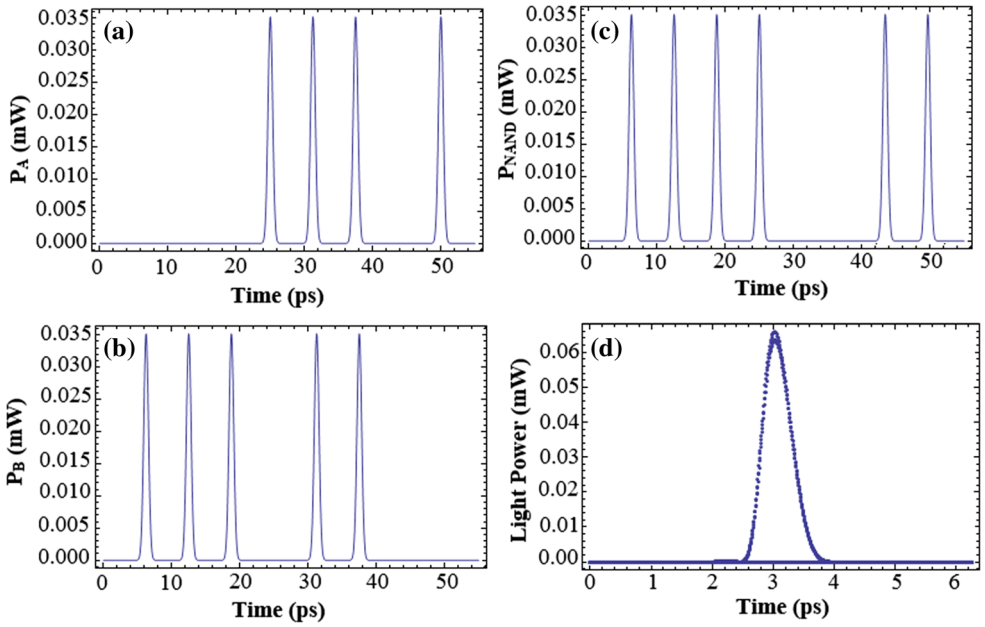

Fig. 3 Simulation results for logical outcome (**c**) and eye diagram (**d**) of NAND operation between data signals A (**a**) and B (**b**) at 160 Gb/s. The obtained Q-factor using PCSOAs–MZIs is 18

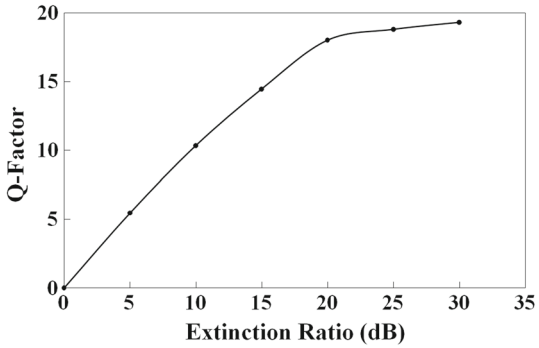

Fig. 4 Q-factor versus inputs signals' extinction ratio

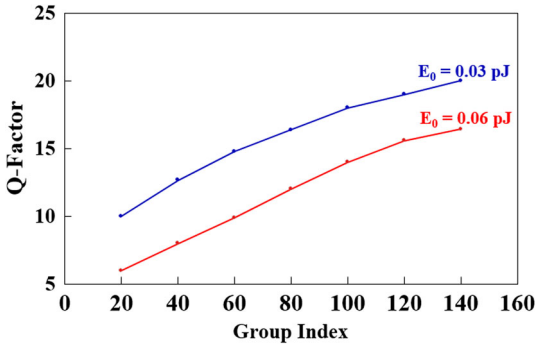

Fig. 5 Q-factor versus PCSOAs' group index for $E_0 = 0.03$ and 0.06 pJ

incur an increased as well as intolerable power penalty at the receiving side [42,43].

The dependence of the Q-factor on the PCSOAs group index (n_g) for $E_0 = 0.03$ and 0.06 pJ is shown in Fig. 5. It can be seen that the Q-factor increases within the entire group index range, while lower pulse energies yield a higher metric value for a given n_g. In both cases, this physically happens because a higher and less saturated PCSOAs gain is enabled [12,44], which favours the achievement of proper switching and accordingly of improved Q-factor.

The Q-factor as a function of the radiation loss (R) of PCSOAs and standard SOAs is shown in Fig. 6. Although the Q-factor variation trend would be expected to be against PCSOAs due to their higher radiation losses over standard SOAs; on the contrary, the Q-factor surpasses that obtained with standard SOAs. This is explained by the fact that these losses are sufficiently compensated in PCSOAs owing to their larger gain attained at much lower bias currents [12].

The variation of the Q-factor against the confinement factor (Γ) of PCSOAs and standard SOAs is shown in Fig. 7. At low values of this parameter, less fraction of the energy of a particular waveguide mode is confined to the active region. This, in turn, impairs the level of available unsaturated gain as well as the amount of signal power that saturates the (PC)SOAs [45], so that eventually it becomes more difficult for the signal to be switched without being degraded and the Q-factor is decreased. Still, the Q-factor is higher for the PCSOAs than for the SOAs for a given Γ because the nonlinear light–matter interactions and the photon density are inherently increased in PCSOAs compared to conventional SOAs [15].

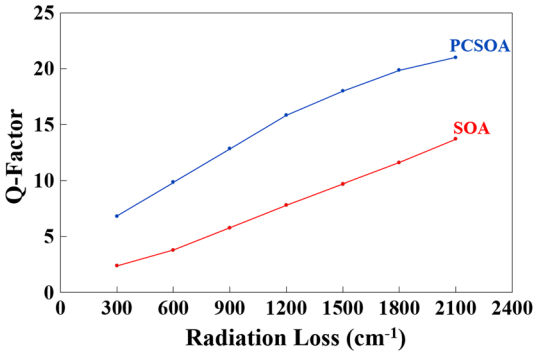

Fig. 6 Q-factor versus radiation loss for PCSOA- and SOA-based NAND operation

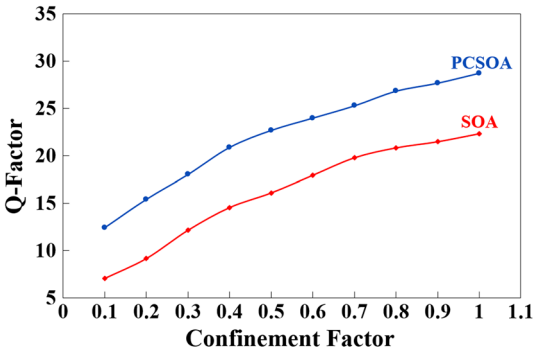

Fig. 7 Q-factor versus confinement factor for PCSOA- and SOA-based NAND operation

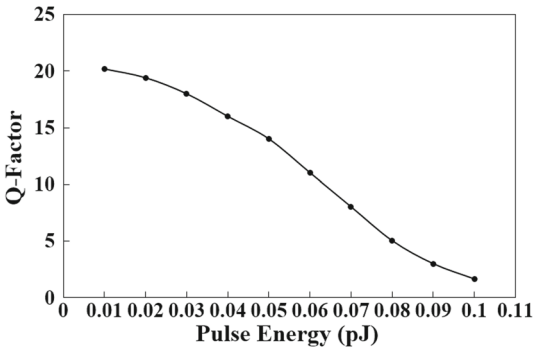

Fig. 8 Q-factor versus input pulse energy

To get a further insight into the performance of the NAND gate, the Q-factor for different input pulse energies is shown in Fig. 8. An increase in the input pulse energy causes a heavier saturation of the PCSOA, which leads to a decrease in the Q-factor. Still, the required switching energy is comparable to that of NAND gates implemented at 160 Gb/s with conventional SOA–MZI. This means that employing PCSOAs in the MZI allows too to render the data pulses sufficient energetic for switching without necessitating to resort to rather complex and inordinately power consuming erbium-doped fibre amplifiers.

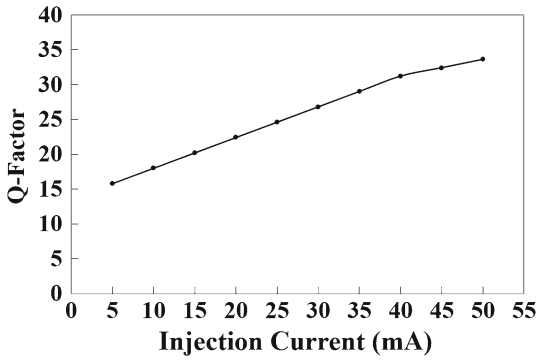

Fig. 9 Q-factor versus PCSOAs' injection current

The free carriers' density increases with the external injection current (I) into the amplifiers active region. This leads to faster gain recovery and hence enhanced PCSOAs dynamic response [46]. As a result, the Q-factor increases with the injection current, as shown in Fig. 9. For conventional SOAs, the dynamic gain perturbation level required for proper switching, which is of the order of 25 dB dictates that $I > 50$ mA, in comparison with $I > 5$ mA for PCSOAs. This difference in the current injection magnitude is attractive from a practical perspective as it implies that the NAND gate can be implemented based on PCSOAs using less complex and power consuming electronic circuitry.

The dependence of the Q-factor on the input signal's pulse width and the PCSOA's carrier lifetime is shown in Fig. 10a, b, respectively. These figures show that the Q-factor decreases with the increase in both pulse width and carrier lifetime. Because wider pulses are more energetic, they cause a stronger saturation of the PCSOAs' gain, which gradually becomes insufficient for proper switching and degrades performance, as shown in Fig. 10a. Since the carrier lifetime determines the speed of gain recovery, the Q-factor becomes higher for smaller values of this parameter, as shown in Fig. 10b. Nevertheless, this metric can be made acceptable for values of both examined parameters, which are affordable by optical pulse generators, in the pulse width case, and nominally available without applying special acceleration techniques, in the carrier lifetime case.

The simulated Q-factor versus the saturation power and the traditional linewidth enhancement factor (α-factor) for a PCSOA and a conventional SOA are shown in Fig. 11a, b, respectively. Figure 11a shows that the Q-factor inclines with increasing the saturation power for both PCSOA and SOA. The Q-factor for PCSOA-based MZI is higher than for SOA-based MZI for the same saturation power owing to the inherently stronger light–matter interaction in PCSOAs [15]. Therefore, from a power-wise perspective, PCSOAs are more efficient for use as nonlinear elements in AOLGs. Figure 11b shows that the Q-factor increases with increasing α-factor. Because the integrated gain response is more enhanced for

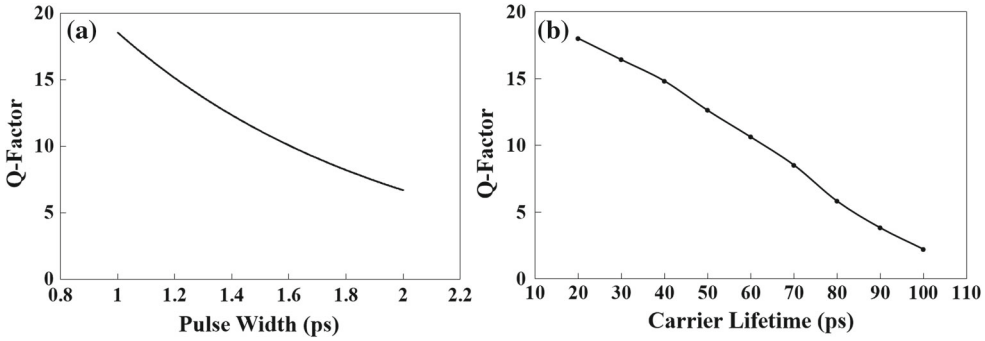

Fig. 10 Q-factor versus **a** pulse width and **b** PCSOAs' carrier lifetime

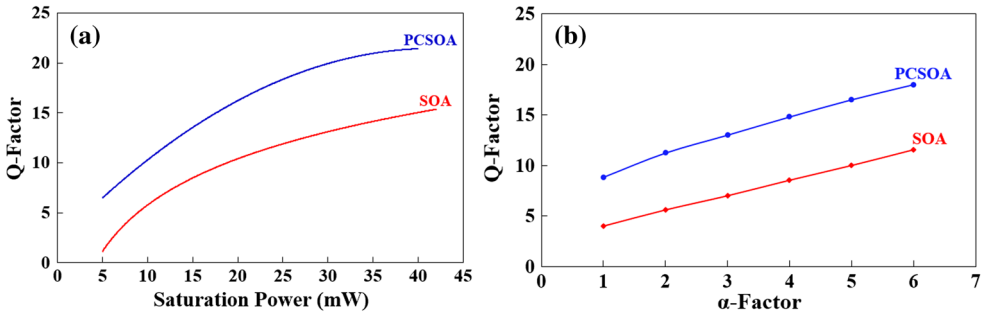

Fig. 11 Q-factor versus **a** saturation power and **b** traditional linewidth enhancement factor (α-factor) for PCSOA- and conventional SOA-based NAND operation

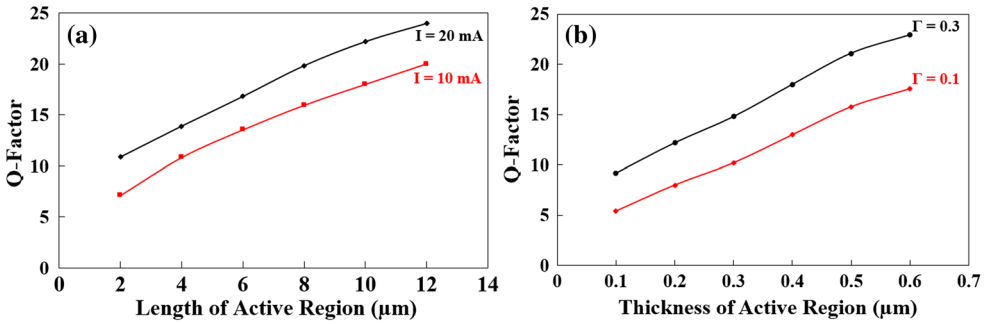

Fig. 12 Q-factor versus PCSOAs' active region **a** length, for $I = 10$ and 20 mA and **b** thickness, for $\Gamma = 0.1$ and 0.3

the PCSOAs than SOAs, the necessary phase shift can be incurred more efficiently in PCSOAs than in SOAs. The performance of the NAND gate using PCSOAs is acceptable for a smaller α-factor compared to conventional SOAs. Since the α-factor depends on the operating conditions [47], and in particular on the relative position of the amplifier gain peak and the signal wavelengths, this implies that the requirements with regard to the PCSOA device fabrication and signal driving can be less stringent.

Figure 12a, b, which have been obtained after making numerical adjustments with regard to the PCSOAs injection current and confinement factor similar to [17], shows that although the Q-factor increases for longer and thicker PCSOAs, yet, because of the enhanced light–matter interaction, these dimensions correspond to a total size which is smaller than if conventional SOAs were used. This result complies with that derived in [17] and indicates that PCSOA-based AOLG schemes can be made more compact than their SOA-based counterparts and hence be favourably amenable to integration.

The PCSOAs amplified spontaneous emission (ASE) is undesirable, as it distorts the profile of the switched pulses. The effect of ASE on the Q-factor has been accounted for by numerically adding it to the power of the NAND output, using the following formula [48,49]:

$$P_{\mathrm{ASE}} = N_{\mathrm{sp}} \left[2\pi\hbar \left(\mathrm{G}_0 - 1\right)\right] \upsilon B_0 \tag{10}$$

where N_{sp} is the spontaneous emission factor and B_0 is the optical bandwidth. A larger ASE increases the intensity level

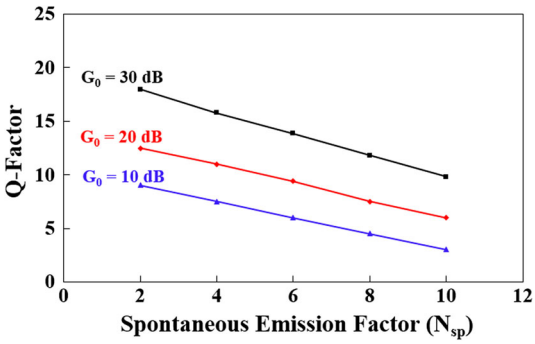

Fig. 13 Q-factor versus PCSOAs' spontaneous emission factor (N_{sp}) for $G_0 = 10$, 20 and 30 dB

of '0's, while it perturbs the level of '1's and hence reduces the Q-factor. The Q-factor versus N_{sp}, for $G_0 = 10$, 20, 30 dB and $B_0 = 3$ nm, $\upsilon = 190$ THz, is shown in Fig. 13. From this figure, it can be deduced that the PCSOAs must provide at least a medium gain to keep the Q-factor acceptable even in the presence of pronounced ASE, which is well within their technological capabilities. On the other hand, a low spontaneous emission factor is preferable, but the detailed experimental characterization of PCSOAs subject to ASE is required to reveal to what extent this would be technologically possible.

4 Conclusion

In conclusion, the performance of an all-optical NAND gate implemented by employing properly configured and connected photonic crystal semiconductor optical amplifiers (PCSOA)-assisted Mach–Zehnder interferometers was theoretically analysed at 160 Gb/s The dependence of the quality factor (Q-factor) on the input signals' and PCSOA critical parameters was assessed with the impact of amplified spontaneous emission included so as to obtain realistic results. This investigation revealed that the Q-factor can be as high as 18, which is well over the lower limit of this metric (> 6) for acceptable performance. The obtained results showed that the Q-factor increases with the group index, radiation loss, injection current, saturation power, α-factor, and active region length and thickness, while it is reduced with the input pulse energy. Also, the Q-factor becomes higher for smaller pulse width and carrier lifetime. The main outcome of the conducted study is that embedding and exploiting in interferometric configurations PCSOAs as nonlinear elements is more efficient for executing fundamental all-optical Boolean logic functions at ultra-high data rates than when using for the same purpose conventional SOAs.

References

[1] Bogoni, A., Potì, L., Ghelfi, P., Scaffardi, M., Porzi, C., Ponzini, F., Meloni, G., Berrettini, G., Malacarne, A., Prati, G.: OTDM-based optical communications networks at 160 Gbit/s and beyond. Opt. Fiber Technol. **13**, 1–12 (2007)

[2] Qin, C., Zhao, J., Yu, H., Zhang, J.: Gain recovery dynamics in semiconductor optical amplifiers with distributed feedback grating under assist light injection. Opt. Eng. **55**, 076116 (2016)

[3] Kumar, Y., Shenoy, M.R.: Enhancement in the gain recovery of a semiconductor optical amplifier by device temperature control. Pramana J. Phys. **87**, 1–6 (2016)

[4] Kumar, Y., Shenoy, M.R.: A novel scheme of optical injection for fast gain recovery in semiconductor optical amplifier. IEEE Photonics Technol. Lett. **26**, 933–936 (2014)

[5] Li, C., Tian, X., Xiu, Z., Shang, Z., Xiao, G., Xiao, T., Yong, L.: Theoretical analysis of ultra-fast phase recovery in semiconductor optical amplifiers. Chin. Sci. Bull. **57**, 1078–1082 (2012)

[6] Ginovart, F., Simon, J.C., Valiente, I.: Gain recovery dynamics in semiconductor optical amplifier. Opt. Commun. **199**, 111–115 (2011)

[7] Giller, R., Manning, R.J., Talli, G., Webb, R.P., Adams, M.J.: Analysis of the dimensional dependence of semiconductor optical amplifier recovery speeds. Opt. Express **15**, 1773–1782 (2007)

[8] Giller, R., Manning, R.J., Cotter, D.: Gain and phase recovery of optically excited semiconductor optical amplifiers. IEEE Photonics Technol. Lett. **18**, 1061–1063 (2006)

[9] Rendon-Salgado, I., Gutierrez-Castrejon, R.: 160 Gb/s all-optical AND gate using bulk SOA turbo-switched Mach-Zehnder interferometer. Opt. Commun. **399**, 77–86 (2017)

[10] Marwaha, A.L.: Reconfiguration of optical logic gates at 160 Gb/s based on SOA-MZI. Comput. Electron. **15**, 1473–1483 (2016)

[11] Marwaha, A.L.: Implementation of optical logic gates at 160 Gbps using nonlinear effect of single SOA. Opt. Laser Technol. **70**, 112–118 (2015)

[12] Mizuta, E., Watanabe, H., Baba, T.: All semiconductor low-Δ photonic crystal waveguide for semiconductor optical amplifier. Jpn. J. Appl. Phys. **45**, 6116–6120 (2006)

[13] Taleb, H., Abedi, K.: Modeling and design of photonic crystal quantum-dot semiconductor optical amplifiers. IEEE Trans. Electron. Devices **61**, 2419–2423 (2014)

[14] Zhang, Y., Zheng, W., Aiyi, Q., Qu, H., Peng, H., Xie, S., Chen, L.: Design of photonic crystal semiconductor optical amplifier with polarization independence. Lightwave Technol. **28**, 3207–3211 (2010)

[15] Taleb, H., Abedi, K.: Optical gain, phase, and refractive index dynamics in photonic crystal quantum-dot semiconductor optical amplifiers. IEEE J. Quantum Electron. **50**, 605–612 (2014)

[16] Taleb, H., Abedi, K.: Design of a novel low power all-optical NOR gate using photonic crystal quantum-dot semiconductor optical amplifiers. Opt. Lett. **39**, 6237–6241 (2014)

[17] Kotb, A., Zoiros, K.E.: Performance analysis of all-optical XOR gate with photonic crystal semiconductor optical amplifier-assisted Mach-Zehnder interferometer at 160 Gb/s. Opt. Commun. **402**, 511–517 (2017)

[18] Mano, M.M., Ciletti, M.D.: Digital Design, 4th edn. Prentice Hall, New Jersey (2006)

[19] Jung, Y.J., Son, C.W., Jhon, Y.M., Lee, S., Park, N.: One-level simplification method for all-optical combinational logic circuits. IEEE Photonics Technol. Lett. **20**, 800–802 (2008)

[20] Li, W., Ma, S., Hu, H., Dutta, N.K.: All-optical latches using quantum-dot semiconductor optical amplifier. Opt. Commun. **285**, 5138–5143 (2012)

[21] Hamilton, S.A., Robinson, B.S.: 40-Gb/s all-optical packet synchronization and address comparison for OTDM networks. IEEE Photonics Technol. Lett. **14**, 209–211 (2002)
[22] Villafranca, A., Cabezón, M., Izquierdo, D., Martínez, J.J., Garcés, I.: Programmable all-optical logic gates based on semiconductor optical amplifiers. In: Proceedings of the International Conference Transparent Optical Networks (ICTON), paper We.B5.6 (2011)
[23] Dutta, N.K., Wang, Q.: Semiconductor Optical Amplifiers, 2nd edn. World Scientific Publishing Company, Singapore (2013)
[24] Kim, J.Y., Kang, J.M., Kim, T.Y., Han, S.K.: All-optical multiple logic gates with XOR, NOR, OR, and NAND functions using parallel SOA-MZI structures: theory and experiment. Lightwave Technol. **24**, 3392–3399 (2006)
[25] Saharia, A., Sharma, R.: An approach for realization of all-optical NAND gate using nonlinear effect in SOA. Int. J. Signal Proc. Imaging Eng. **1**, 13–17 (2014)
[26] Ye, X., Ye, P., Zhang, M.: All-optical NAND gate using integrated SOA-based Mach-Zehnder interferometer. Opt. Fiber Technol. **12**, 312–316 (2006)
[27] Kotb, A., Ma, S., Chen, Z., Dutta, N.K., Said, G.: All-optical logic NAND based on two-photon absorption in semiconductor optical amplifiers. Opt. Commun. **283**, 4707–4712 (2010)
[28] Kotb, A., Ma, S., Chen, Z., Dutta, N.K., Said, G.: All-optical logic NAND based on two-photon absorption. In: Proceedings of the SPIE Photon. Fiber and Crystal Devices: Advances in Materials and Innovations in Device Applications IV, 77810D (2010)
[29] Kotb, A., Ma, S., Chen, Z., Dutta, N.K., Said, G.: Effect of amplified spontaneous emission on semiconductor optical amplifier based all-optical logic. Opt. Commun. **284**, 5798–5803 (2011)
[30] Son, C.W., Kim, S.H., Jhon, Y.M., Byun, Y.T., Lee, S., Woo, D.H., Kim, S.K., Yoon, T.H.: Realization of all-optical XOR, NOR, and NAND gates in a single format by using semiconductor optical amplifiers. Jpn. J. Appl. Phys. **46**, 232–234 (2007)
[31] Kim, S.H., Kim, J.H., Choi, J., Woo, D.H.: All-optical NAND gate using cross-gain modulation in semiconductor optical amplifiers. Electron. Lett. **2**, 957–959 (2005)
[32] Chattopadhyay, T.: All-optical programmable Boolean logic unit using semiconductor optical amplifiers on the Mach-Zehnder interferometer arms switch. IET Optoelectron. **5**, 270–280 (2011)
[33] Cao, T., Ho, Y.L.D., Heard, P.J., Barry, L.P., Kelly, A.E., Cryan, M.J.: Fabrication and measurement of a photonic crystal waveguide integrated with a semiconductor optical amplifier. J. Opt. Soc. Am. B **26**, 768–777 (2009)
[34] Kotb, A., Maeda, J.: NXOR based on semiconductor optical amplifiers with the effect of amplified spontaneous emission. Optoelectron. Lett. **8**, 437–440 (2012)
[35] Kotb, A.: Simulation of all-optical logic NOR gate based on two-photon absorption with semiconductor optical amplifier-assisted Mach-Zehnder interferometer with the effect of amplified spontaneous emission. Korean Phys. Soc. **66**, 1593–1598 (2015)
[36] Kotb, A.: Modeling of high-quality-factor XNOR gate using quantum-dot semiconductor optical amplifiers at 1 Tb/s. Braz. J. Phys. **45**, 288–295 (2015)
[37] Ma, S., Sun, H., Chen, Z., Dutta, N.K.: High speed all-optical PRBS generation based on quantum-dot semiconductor optical amplifiers. Opt. Express **17**, 18469–18477 (2009)
[38] Singh, P., Tripathi, D.K., Jaiswal, S., Dixit, H.K.: Design and analysis of all-optical AND, XOR and OR gates based on SOA-MZI configuration. Opt. Laser Technol. **66**, 35–44 (2015)
[39] Singh, S., Kaur, R., Kaler, R.S.: Photonic processing for all-optical logic gates based on semiconductor optical amplifier. Opt. Eng. **53**, 116102 (2014)
[40] Essiambre, R.J., Raybon, G., Mikkelsen, B.: Pseudo-linear transmission of high-speed TDM signals: 40 and 160 Gb/s. In: Kaminow, I.P., Li, T. (eds.) Optical Fiber Telecommunications IV-B: Systems and impairments. Academic Press, Cambridge (2002)
[41] Weber, H.G., Nakazawa, M.: Ultrahigh-Speed Optical Transmission Technology. Springer, Berlin (2007)
[42] Ishikawa, H.: Ultrafast All-Optical Signal Processing Devices. Wiley, London (2008)
[43] Cvijetic, M., Djordjevic, I.B.: Advanced Optical Communication Systems and Networks. Artech House, Norwood (2013)
[44] Zoiros, K.E., Vardakas, J., Houbavlis, T., Moyssidis, M.: Investigation of SOA-assisted Sagnac recirculating shift register switching characteristics. Optik **116**, 527–541 (2005)
[45] Bonk, R., Vallaitis, T., Guetlein, J., Meuer, C., Schmeckebier, H., Bimberg, D., Koos, C., Freude, W., Leuthold, J.: The input power dynamic range of a semiconductor optical amplifier and its relevance for access network applications. IEEE Photonics **3**, 1039–1053 (2011)
[46] Ueno, Y., Nakamura, S., Tajima, K.: Nonlinear phase shifts induced by semiconductor optical amplifiers with control pulses at repetition frequencies in the 40–160-GHz range for use in ultrahigh-speed all-optical signal processing. J. Opt. Soc. Am. B **19**, 2573–2589 (2002)
[47] Schares, L., Schubert, C., Schmidt, C., Weber, H.G., Occhi, L., Guekos, L.: Phase dynamics of semiconductor optical amplifiers at 10–40 GHz. IEEE J. Quantum Electron. **39**, 1394–1408 (2003)
[48] Kotb, A.: All-Optical Logic Gates Using Semiconductor Optical Amplifier. Lambert Academic Publishing, Saarbrucken (2012)
[49] Melo, A.M., Petermann, K.: On the amplified spontaneous emission noise modeling of semiconductor optical amplifiers. Opt. Commun. **281**, 4598–4605 (2008)

Amer Kotb has obtained the Ph.D. and M.Sc. in Electronics in 2012 and 2006, respectively. His Ph.D. researches are carried out at the Connecticut University, Connecticut, USA. He is an Associate Professor in Changchun Institute of Optics, Fine Mechanics, and Physics, Changchun 13003, China. Also, he is as Associate Professor at Fayoum University, Faculty of Science, Department of Physics, Fayoum 63514, Egypt. Amer has published more than 30 journal papers as the first author and one book in semiconductor optical amplifier (SOA)-based all-optical logic gates. His research is in the area of optoelectronic devices and telecommunication systems. Current research activities are investigation of: soliton all-optical logic devices with SOAs, photonic crystal circuits operating at high data rate, reflective SOAs, and graphene SOAs.

Kyriakos E. Zoiros has received the Diploma of Electrical and Computer Engineering from the National Technical University of Athens, Athens, Greece, in 1996, where he received the Ph.D. degree in optical communications from the Photonics Communications Research Laboratory in 2000. He is currently an Associate Professor of optical communications in the Department of Electrical and Computer Engineering, Democritus University of Thrace, Xanthi, Greece. In spring 2009, he was on leave at the University of Limerick in Ireland doing experimental work on semiconductor optical amplifier (SOA) pattern effect suppression techniques at the Optical Communications Research Group. He is the author or coauthor of more than 60 international journal and conference papers as well as of three book chapters. His current research interests include conventional as well as quantum-dot SOA devices, circuits and subsystems, applications of microring resonators in optical communications, microwave photonics, and free space optical communications.

Chunlei Guo is the director of the Guo China-US Photonics Laboratory in Changchun Institute of Optics, Fine Mechanics, and Physics, Changchun 13003, China. Prof. Guo's research interests focus on laser–matter interactions at high intensities, nano-photonics, femtosecond laser surface nano- and microstructuring, and surface plasmonics. He and his coworkers invented the so-called black and coloured metals, which have a broad range of technological applications and have been covered extensively by the media. He is an elected Fellow for American Physical Society, Optical Society of America, and international Academy of Photonics and Laser Engineering. He serves as an Editor and on editorial boards for a number of scientific journals and is the past Chair of Short-Wavelength and High-Field Physics Group in the Optical Society of America.